Supporting Information

Rate Law for Photoelectrochemical Water Splitting over CuO

Bo-Yuan Gao, Wen-Hua Leng*

Department of Chemistry, Zhejiang University, Hangzhou, Zhejiang, 310058, China

Table of Contents

1. Material Characterizations

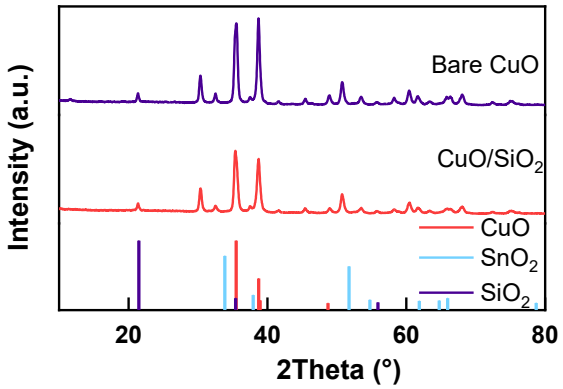

Fig. S1. XRD patterns of the bare CuO and CuO/SiO_2 electrodes.

2. Effect of spin-coating layer on the photoelectrochemical performance

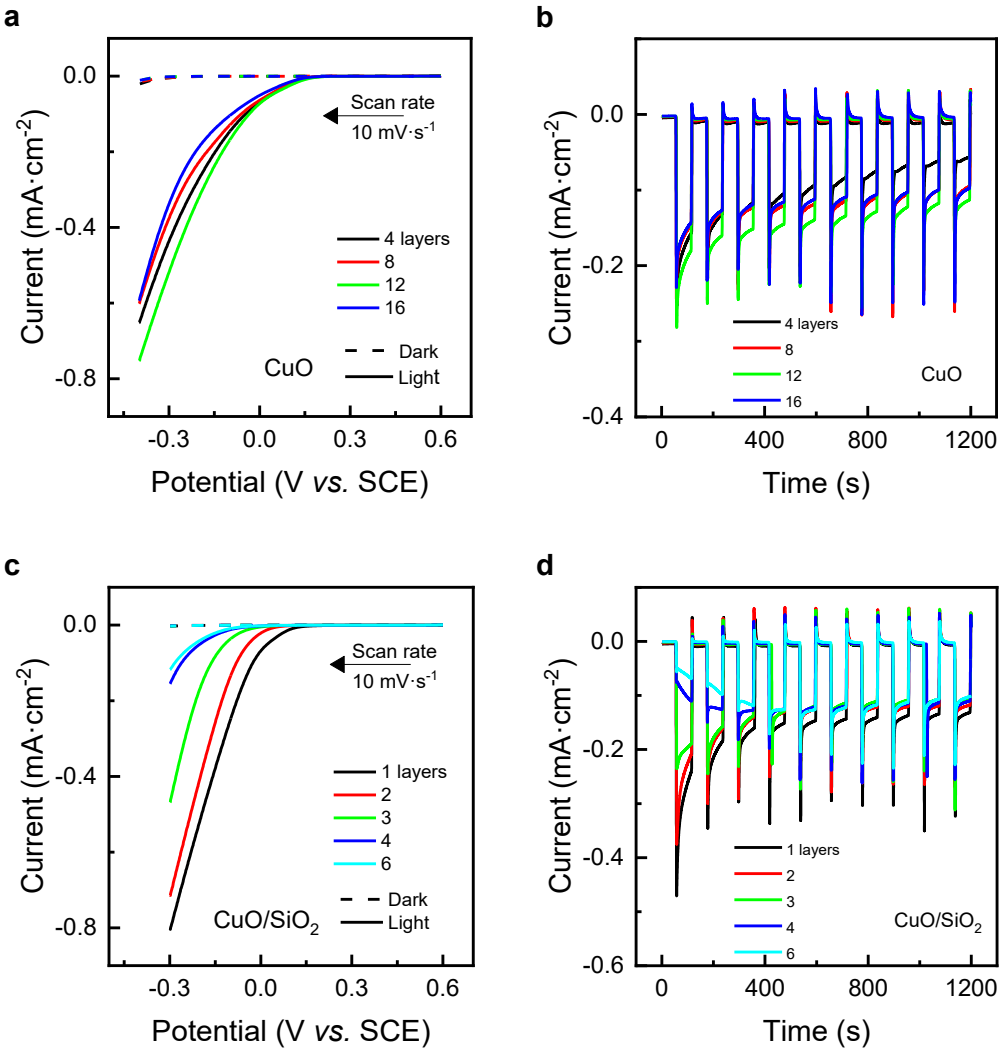

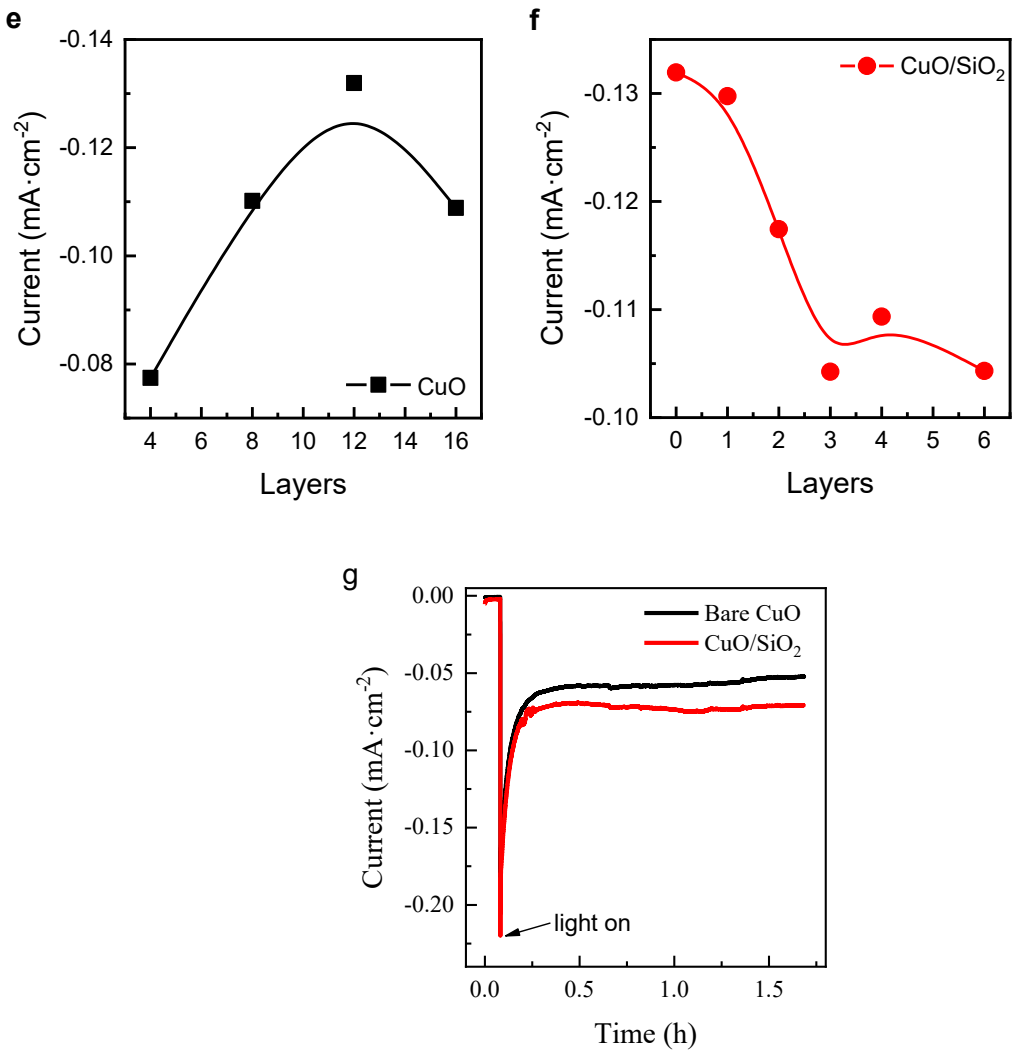

Fig. S2. The effect of film thickness (layers) on the photoelectrochemical performance of the electrodes. I-V curves in the dark and under white illumination for (a) CuO and (c) CuO electrodes with SiO_2 modification (CuO/SiO_2); the corresponding I-t curves at -0.2 V_{SCE} under illumination: (b) CuO and (d) CuO/SiO_2 electrodes; (e) the spin-coating layer-dependence of photoelectrochemical performance for CuO electrodes; (f) photocurrent as a function of SiO_2 coating layer for CuO electrodes; (g) stability plots of CuO and CuO/SiO_2 electrodes after testing under illumination at –0.2 V_{SCE}.

3. Steady-state photocurrent at various light intensities

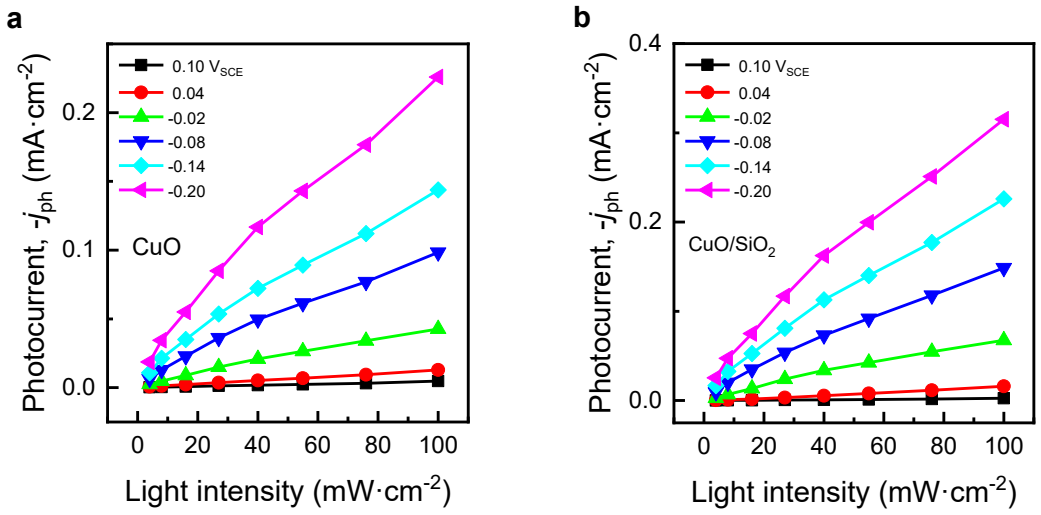

Fig. S3. The photocurrent at applied potentials indicated, as a function of light intensity for (a) CuO and (b) CuO/SiO₂ electrodes.

4. Measurement of surface states

The characteristics of the surface states were investigated by EIS as reported previously [1–5]. The impedance responses due to filling and emptying of the interface states give rise to an additional response Z_{SS}. The measured Z_{SS} is consisted of electrolyte resistance R_S and a serial pseudo-capacitance C_p, which is the response of interface states. The total measured capacitance is simply the sum of C_p and C_{SC}, which can be obtained from real and imaginary parts of the measured impedance *Re*(Z) and *Im*(Z), respectively, as described by Eqs. S1 and S2.

$$C_p = [\omega Im(Z)(1 + D^2)]^{-1} \quad \text{(S1)}$$

$$D = [Re(Z) - R_s]/[-Im(Z)] \quad \text{(S2)}$$

According to previous reports [1–5], the different positions of the capacitance peak may involve diverse surface states and the height of the capacitance peak represents the density of the surface states. The curve of applied potential and parallel capacitance (C_p-E) can be used to distinguish various surface states. Similar to the Mott-Schottky analysis, the impedance due to surface states was measured by performing a potential scan from positive to negative (0.1~–0.4 V_{SCE}) with a step of 50 mV at a fixed frequency with a sinusoidal amplitude of 3 mV.

The results in the C_p-E curves of CuO and CuO/SiO$_2$ electrodes in the dark and under illumination after subtraction of space charge component are shown in Fig. S4. The appearance of one peak at ~0 V_{SCE} is observed for both electrodes in the

dark and under illumination, stating that a surface state locates at the energy level of ~0 V_{SCE}. Besides, the height of the capacitance peak is increased significantly under illumination for both electrodes, indicating that the photogenerated intermediates can be stored in these surface states. Furthermore, the peak height of the CuO/SiO_2 electrode under illumination is much greater than that of the CuO electrode, implying greater accumulation of electron at the electrode surface. This is in consistent with the greater surface charge density of the CuO/SiO_2 electrode as shown in Figure 3.

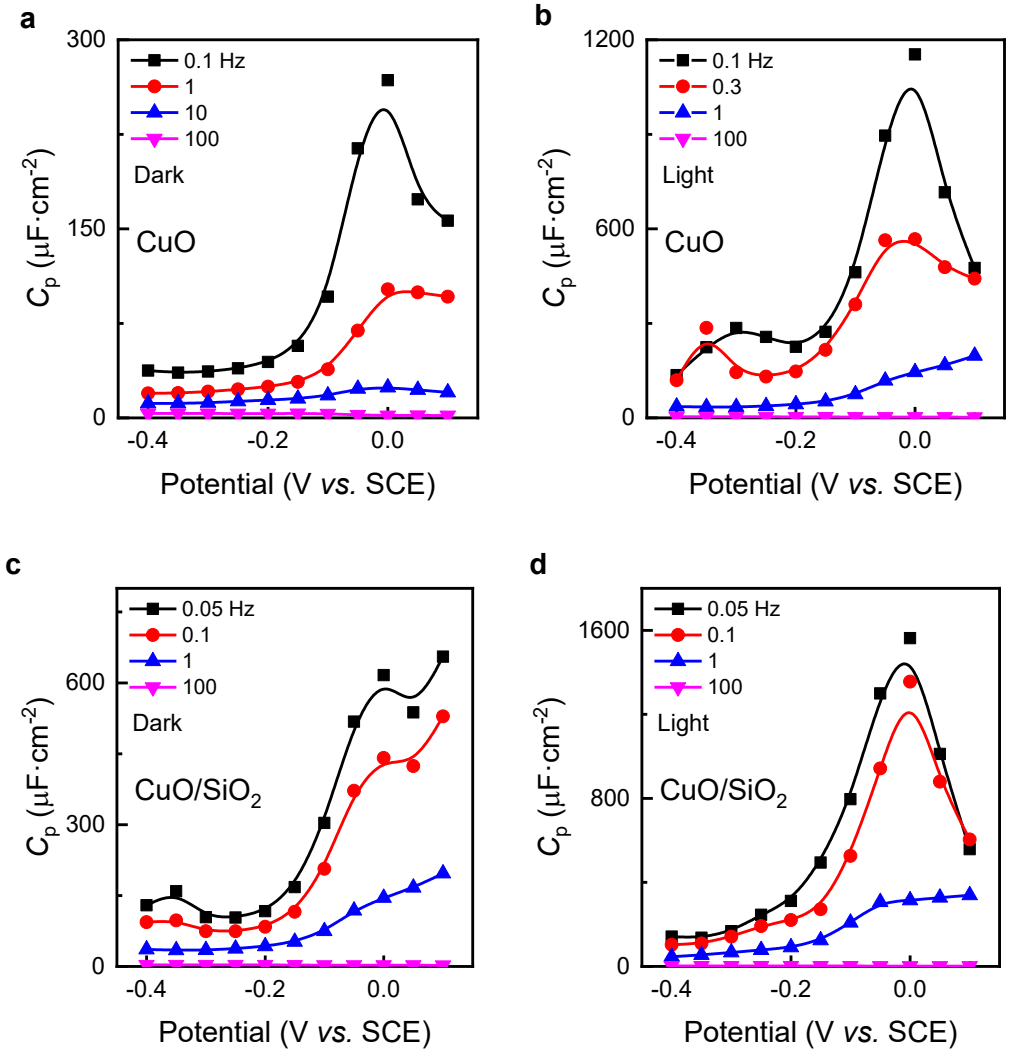

Fig. S4. C_p-E curves of CuO and CuO/SiO_2 electrodes in the dark and under illumination (100 mW·cm^{-2}) for the CuO electrodes (a) in the dark and (b) under illumination; and the CuO/SiO_2 electrodes (c) in the dark and (d) under illumination.

5. Photogenerated surface charge at various light intensities

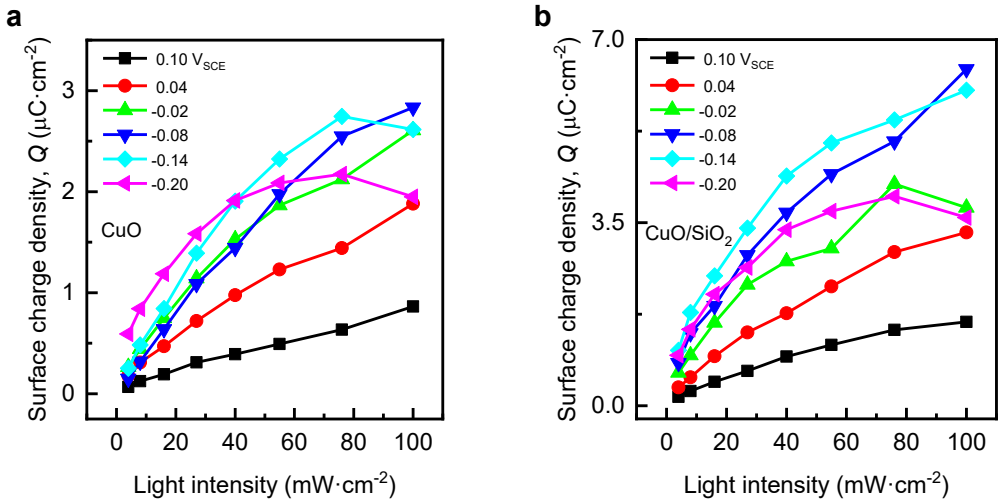

Fig. S5. The surface charge density plots at the indicated applied potential and under different light intensities for (a) CuO and (b) CuO/SiO₂ electrodes.

6. EIS response of CuO photoelectrodes

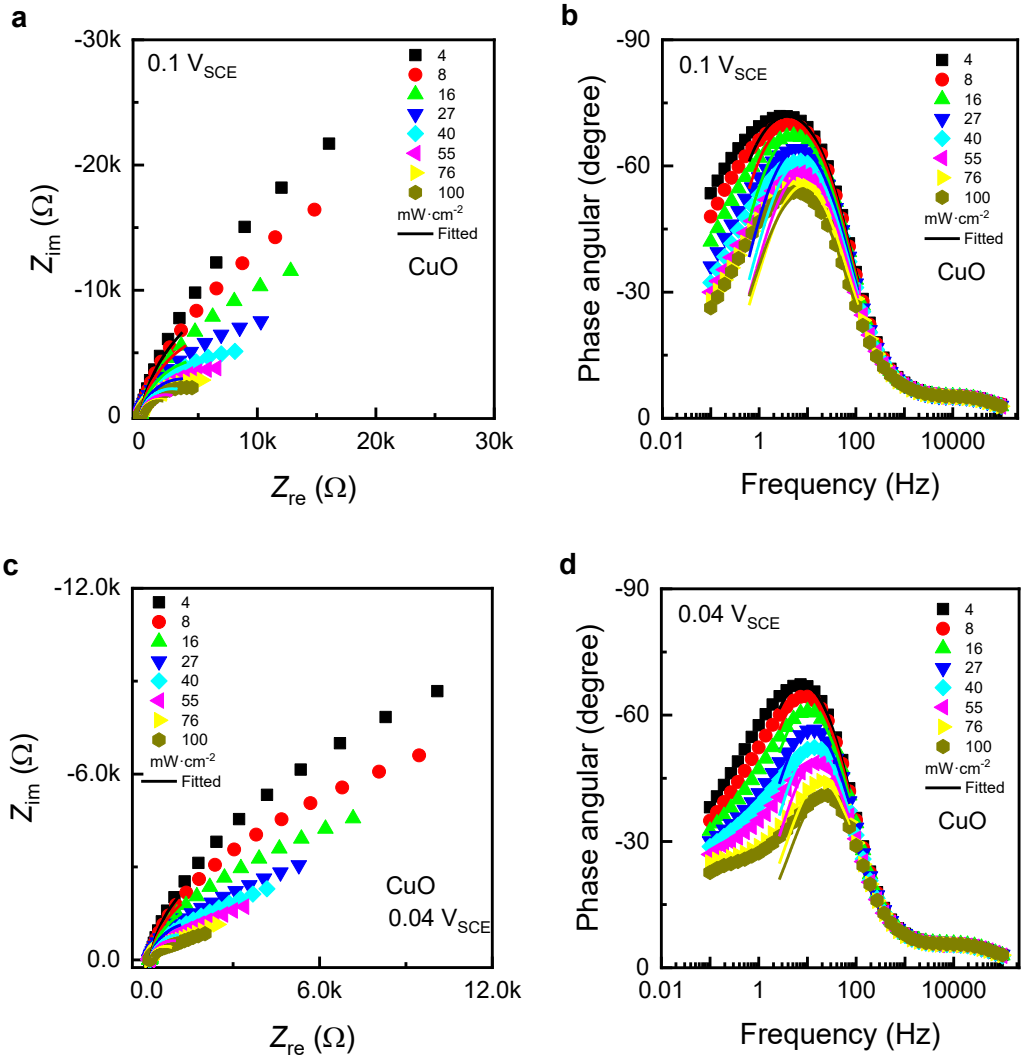

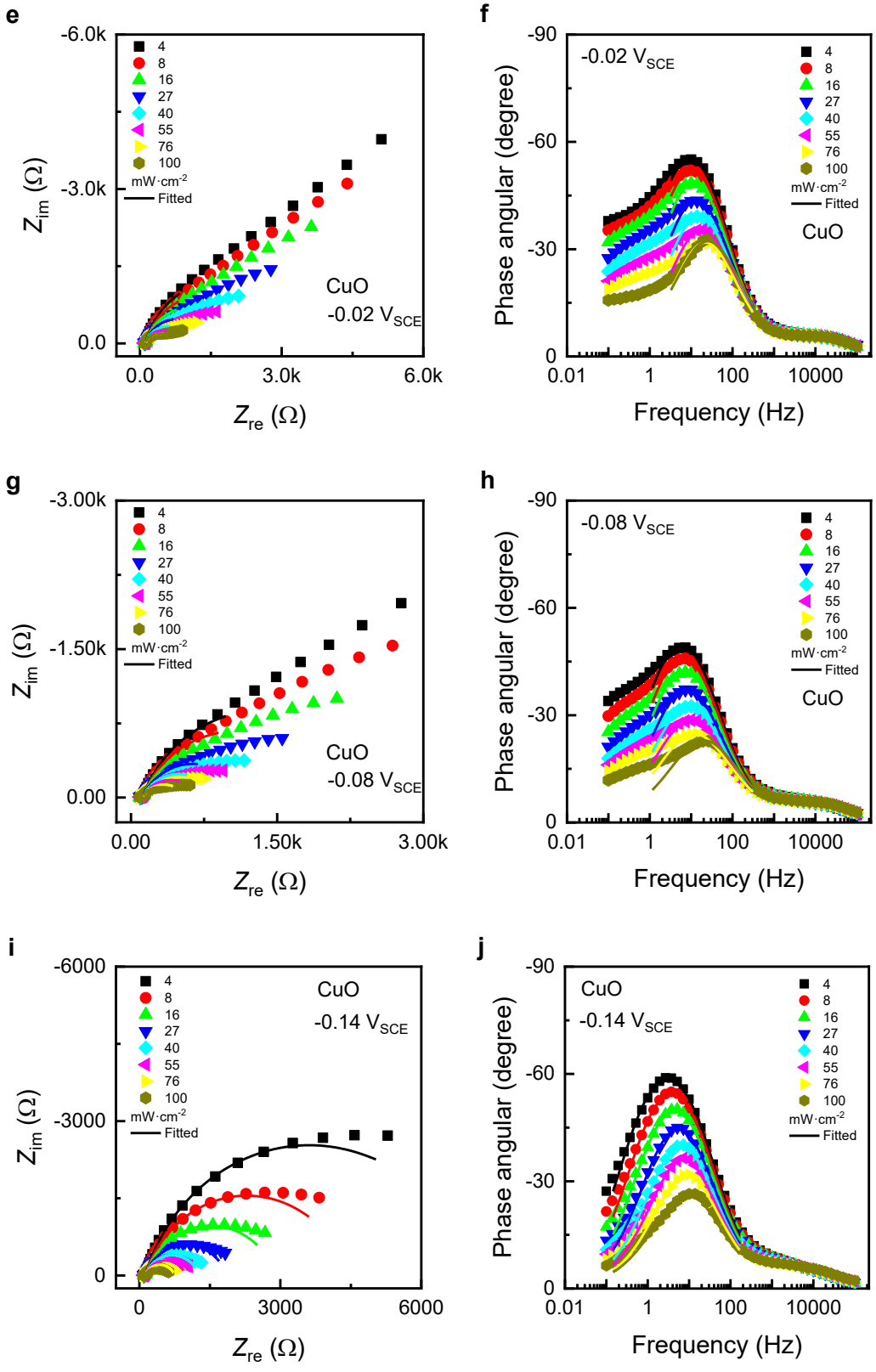

Fig. S6. EIS responses at various potentials and light intensities indicated for the CuO electrodes: Nynquist plots: (a), (c), (e), (g) and (i); Bode plots: (b), (d), (f), (h) and (j).

7. EIS response of CuO/SiO_2 photoelectrodes

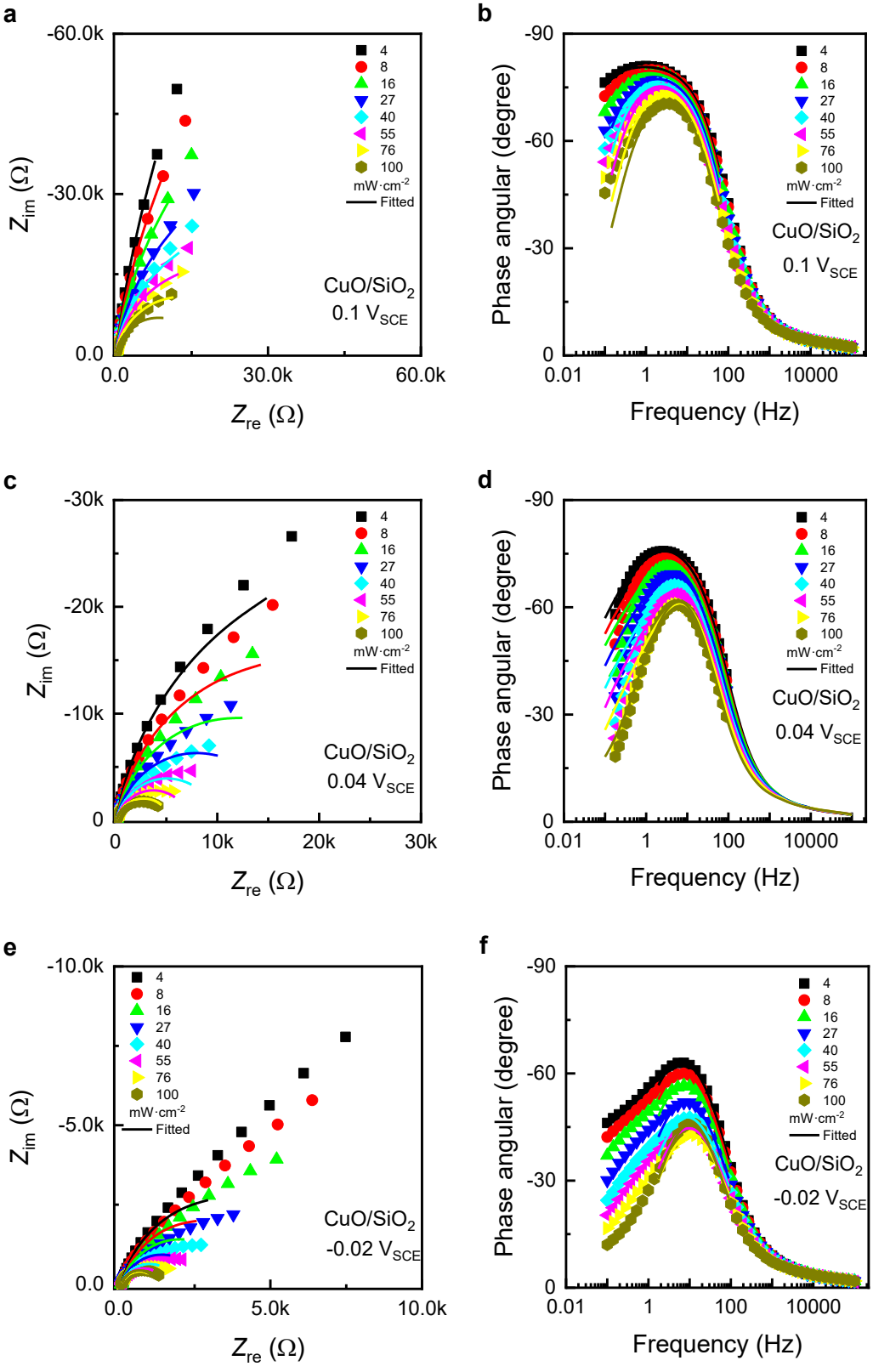
a
-60.0k
-30.0k
0.0
0.0
30.0k
60.0k
Z_{im} (Ω)
Z_{re} (Ω)
4
8
16
27
40
55
76
100
mW·cm^{-2}
Fitted
CuO/SiO$_2$
0.1 V$_{SCE}$
b
-90
-60
-30
0
0.01
1
100
10000
Phase angular (degree)
Frequency (Hz)
c
-30k
-20k
-10k
0
0
10k
20k
30k
d
e
-10.0k
-5.0k
5.0k
10.0k
CuO/SiO$_2$
-0.02 V$_{SCE}$
f

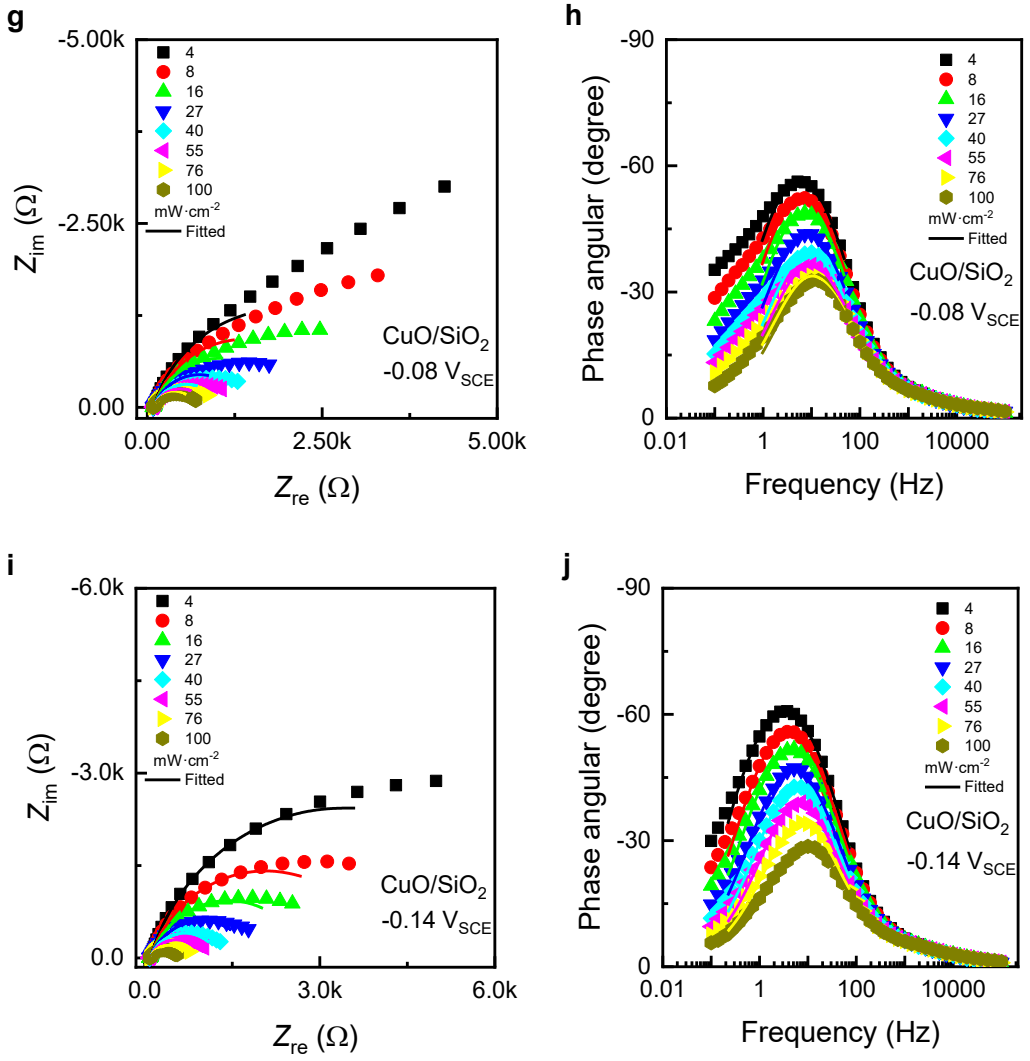

Fig. S7. EIS responses at various potentials and light intensities indicated for the CuO/SiO₂ electrodes: Nynquist plots: (a), (c), (e), (g) and (i); Bode plots: (b), (d), (f), (h) and (j).

8. Charge density-dependence of characteristic angular frequency ω^1_{max}

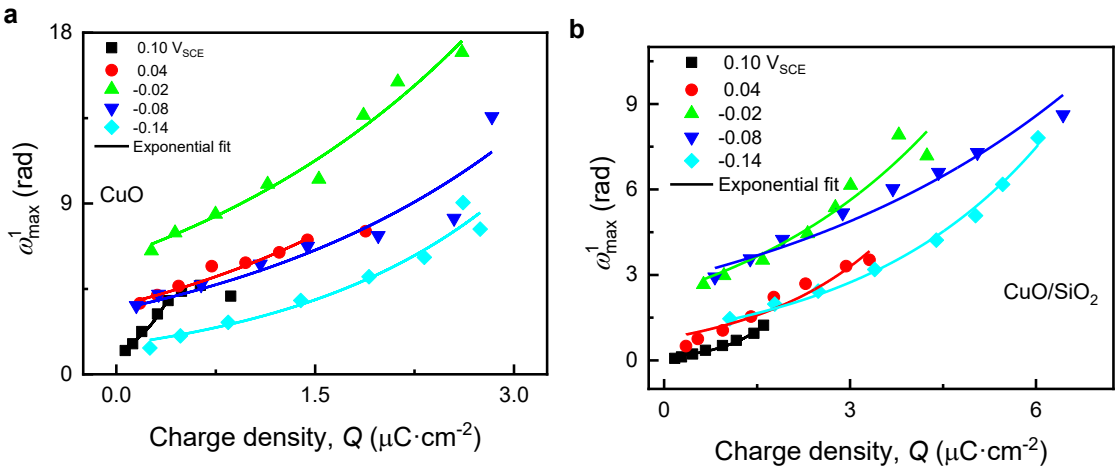

Fig. S8. Relationship of the k_{ct} (ω^1_{max}) and the surface charge density Q at different applied potentials. (a) CuO electrode, (b) CuO/SiO₂ electrode.

9. Rate law for CuO electrode with 3 layers of SiO_2

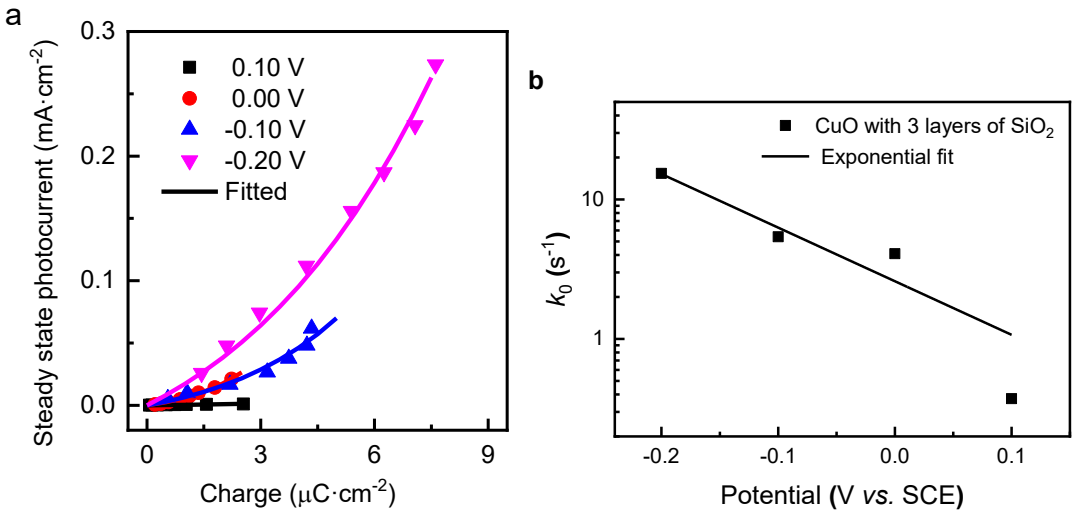

Fig. S9. (a) The reactant concentration dependence of the rate law in terms of photocurrent (J_{ph} vs. Q) for the CuO electrodes with 3 layers of SiO_2; (b) relationship between k_0 and applied potential.

Table S1. Rate equations for photoelectrochemical water splitting over CuO with 3 layers of SiO_2.

Applied potential/V_{SCE}	CuO with 3 layers of SiO_2
0.1	$J_{ph} = -0.37 * \exp(0.11 * [e_s]) * [e_s]$
0.0	$J_{ph} = -4.09 * \exp(0.38 * [e_s]) * [e_s]$
-0.1	$J_{ph} = -5.41 * \exp(0.19 * [e_s]) * [e_s]$
-0.2	$J_{ph} = -15.37 * \exp(0.11 * [e_s]) * [e_s]$

10. Comparison with the relevant literatures

In literature [6], the value of n was obtained through simultaneously measured J_{ph}^{st} and $[e]_s^{st}$ with the assumption that k_{ct} is a constant. Similar rate law analyses have been reported for the water photo-oxidation on several metal oxide semiconductors[7–10] (see Table S2). However, this analysis is questionable, since the assumption is not justified independently and k_{ct} is proofed to be surface hole density dependent [11, 12].

On the contrary, in our study, each kinetic parameter for the rate expression was independently obtained. The correlation between the product of k_{ct} and $[e]_s^{st}$ with the measured J_{ph}^{st} at the given potentials demonstrates the validity of our rate equation (see Fig. 5a and b). In particular, it is found that the $k$ct is exponentially dependent on the surface electron density as described by *Eq. 8* (see Fig. 4e),

which is the key difference between other reports [6–9, 13] and ours (see Table S2). This unconventional phenomenon of a reactant concentration dependent rate constant has been reported for the water photooxidation on several n-type semiconductors and can be explained as follow: The accumulation of such a high concentration photogenerated charge on the electrode surface (10^{13}~10^{14} cm–^{2} for CuO electrodes) will result in the applied potential redistribution between the space charge layer and the Helmholtz layer (*Eq. 7*), and consequently affecting the activation energy for charge transferring across the interface of electrode/electrolyte (*partial Fermi level pinning*). Thus, the surface charge density dependent k_{ct} is observed and the reactant concentration dependence of rate law in terms of photocurrent can be expressed by *Eq. 9*. Additionally, the differential rate equation for the photoelectrochemical water splitting over the Cu_2O/SiO_2 electrodes is determined which, to the best of our knowledge, has not been reported so far, and is another important difference between our work and relevant literatures.

Table S2. The comparison between the rate equation of this work and the results in literatures

Electrode	k_{ct}	Reaction equation	Ref.
CuO (p-type)	$k_{ct} = k_0 \exp(A[e_s])$	$J_{ph} = k_0 \exp(A[e_s])[e_s]$	This work
CuO/SiO_2 (p-type)	$k_{ct} = k_0 \exp(A[e_s])$	$J_{ph} = k_0 \exp(A[e_s])[e_s]$	This work
WO_3 (n-type)	$k_{ct} = k_0 \exp(A[h_s])$	$J_{ph} = k_0 \exp(A[h_s])[h_s]$	[2]
TiO_2 (n-type)	$k_{ct} = k_0 \exp(A[h_s])$	$J_{ph} = k_0 \exp(A[h_s])[h_s]$	[14]
Cu_2O/RuO_X (p-type)	constant	$J_{ph} = k_{ct}([e_s])^2$	[6]
α-Fe_2O_3 (n-type)	constant	$J_{ph} = k_{ct}([h_s])^n$ (n=1 at low charge density; n=3 at high charge density)	[7]
TiO_2 (n-type)	constant	$J_{ph} = k_{ct}([h_s])^n$ (n=2 at pH 0.6 and 6.7; n=3 at pH13.6)	[8]

WO_3 (n-type)	constant	$J_{ph} = k_{ct}([h_s])^n$ (n=1 at low charge density; n=2.5 at high charge density)	[9]
$BiVO_4$ (n-type)	constant	$J_{ph} = k_{ct}([h_s])^n$ (n=1 at low charge density; n=3 at high charge density)	[10]

Note: $[e_s]$ and $[h_s]$ are the surface electron density and surface hole density, respectively, k_{ct} is the charge transfer rate constant, n is the reaction order with respect to charge density, and J_{ph} is the photocurrent. More details please refer to the corresponding references.

References

[1] Oskam G, Schmidt J C, Hoffmann P M, Searson P C. Electrical properties of N-Type (111) Si in aqueous $K_4Fe(CN)_6$ solution: I. interface states and recombination impedance[J]. J. Electrochem. Soc., 1996, 143(8): 2531–2537.

[2] Zhang S F, Gao B Y, Leng W H. Kinetic difference in water photooxidation between TiO_2 and WO_3 electrodes by rate law Analysis[J]. ACS Appl. Energy Mater., 2023, 6(3): 1973–1981.

[3] Zhang S F, Leng W H. Quantitative determination the role of the intrabandgap states in water photooxidation over hematite electrodes[J]. J. Phys. Chem. Lett., 2023, 14(41): 9316–9323.

[4] Cheng X F, Leng W H, Pi O Y, Zhang Z, Zhang J Q, Cao C N. Enhancement of photocatalytic activity of TiO_2 film electrode by in situ photoelectro-generating active chlorine[J]. Trans. Nonferrous Met. Soc. China., 2007, 17(5): 1087–1092.

[5] Leng W H, Zhang Z, Zhang J Q, Cao C N. Investigation of the kinetics of a TiO_2 photoelectrocatalytic reaction involving charge transfer and recombination through surface states by electrochemical impedance spectroscopy[J]. J. Phys. Chem. B, 2005, 109(31): 15008–15023.

[6] Pastor E, Le Formal F, Mayer M T, Tilley S D, Francàs L, Mesa C A, Grätzel M, Durrant J R. Spectroelectrochemical analysis of the mechanism of (photo)electrochemical hydrogen evolution at a catalytic interface[J]. Nat. Commun., 2017, 8(1): 14280.

[7] Le Formal F, Pastor E, Tilley S D, Mesa C A, Pendlebury S R, Grätzel M, Durrant J R. Rate law analysis of water oxidation on a hematite surface[J]. J. Am. Chem. Soc., 2015, 137(20): 6629–6637.

[8] Kafizas A, Ma Y, Pastor E, Pendlebury S R, Mesa C, Francàs L, Le Formal F, Noor N, Ling M, Sotelo-Vazquez C, Carmalt C J, Parkin I P, Durrant J R. Water oxidation kinetics of accumulated holes on the surface of a TiO_2 photoanode: a rate law analysis[J]. ACS Catal., 2017, 7(7): 4896–4903.

[9] Mesa C A, Francas L, Yang K R, Garrido-Barros P, Pastor E, Ma Y, Kafizas A, Rosser T E, Mayer M T, Reisner E, Gratzel M, Batista V S, Durrant J R. Multihole water oxidation catalysis on haematite photoanodes revealed by operando spectroelectrochemistry and DFT[J]. Nat. Chem., 2020, 12(1): 82–89.

[10] Ma Y, Mesa C A, Pastor E, Kafizas A, Francàs L, Le Formal F, Pendlebury S R, Durrant J R. Rate law analysis of water oxidation and hole scavenging on a $BiVO_4$ photoanode[J]. ACS Energy Lett., 2016, 1(3): 618–623.

[11] Peter L M, Walker A B, Bein T, Hufnagel A G, Kondofersky I. Interpretation of photocurrent transients at semiconductor electrodes: Effects of band-edge unpinning[J]. J. Electroanal. Chem., 2020, 872: 114234.

[12] Zhang S F, Leng W H. Questioning the rate law in the analysis of water oxidation catalysis on haematite photoanodes[J]. Nat. Chem., 2020, 12: 1097–1098.

[13] Righi G, Plescher J, Schmidt F P, Campen R K, Fabris S, Knop-Gericke A, Schlögl R, Jones T E, Teschner D, Piccinin S. On the origin of multihole oxygen evolution in haematite photoanodes[J]. Nat. Catal., 2022, 5(10): 888–899.

[14] Zhang S F, Leng W H, Liu K. Unconventional rate law of water photooxidation at TiO_2 electrodes[J]. Phys. Chem. Chem. Phys., 2023, 25(18): 12891–1289